31st Annual International Conference of the IEEE EMBS
Minneapolis, Minnesota, USA, September 2-6, 2009

Intramural Spatial Variation of Optical Tissue Properties Measured with Fluorescence Microsphere Images of Porcine Cardiac Tissue

Ayush Goyal[a], Jeroen van den Wijngaard[b], Pepijn van Horssen[b], Vicente Grau[c], Jos Spaan[b], Nic Smith[a]

[a] Computational Biology, Computing Laboratory, University of Oxford, United Kingdom
[b] Department of Biomedical Engineering and Physics, Academic Medical Center, University of Amsterdam, The Netherlands
[c] Engineering Science and Oxford e-Research Centre, United Kingdom

Abstract—**This proceeding studies the optical fluorescence images of a porcine heart filled with microspheres of two colors, carmine and red. A significant difference in the total optical tissue attenuation coefficient was observed between excitation and emission for both carmine (excitation – 13±4(1/mm) and emission – 9.4±3(1/mm)) and red (excitation - 29±5(1/mm) and emission – 25±5(1/mm)), indicating that optical tissue properties can change significantly for a small change in light wavelength. The above-mentioned large ranges of variation observed in the tissue attenuation coefficient for excitation and emission (both for carmine and red) suggest significant intramural variation of optical properties across the entire organ. Patterns of global spatial variation in optical attenuation properties in tissue across the entire organ were observed. A novel method using fluorescence microsphere images is presented for measurement of the tissue attenuation's intramural variation across an entire organ.**

I. Introduction

LIGHT penetration in tissue has many applications in the medical sciences. It is used for detecting bacterial pathogens in living hosts, measuring neoplasmic tumor growth, pharmacokinetic study of drug effects, photodynamic cancer therapy [1], optical mapping of bioelectric signals [2], and intramural fluorescence imaging of organs [3]. In imaging fluorescent biomarkers, the intensity of the detected fluorescent signal depends upon how many of the photons reach the sensor and this is contingent to the scattering, absorption, and attenuation of the emission light in the tissue.

This paper studies optical fluorescence imaging, which is used for obtaining high-contrast images of coronary vasculature, filled with a fluorescent dye [3]. In order to extract the vasculature from the images, the centerlines and radii of the blood vessels throughout the cryomicrotome data need to be determined, thus allowing reconstructions of coronary networks. However, before the morphology information is extracted, the tissue transparency effects in the form of haloes surrounding large bright vessels, caused by the scattering and distribution of light from fluorescent cast filled in vessels underlying the cutting surface need to be annulled. Replacing the out of focus fluorescence requires knowledge of the spatial variation of optical attenuation properties of the tissue in which the vasculature is embedded.

A. Tissue Optics

The propagation and subsequent attenuation of light through tissue is parameterized by the sum of the absorption μ_a [1/microns] and scattering μ_s [1/microns] coefficients, the total attenuation coefficient μ_t [1/microns], inverse of the mean free path l [microns] of photons [4], which are scattered and absorbed by atoms in the tissue. This is mathematically denoted in equation (1) below [5]:

$$\mu_a+\mu_s=\mu_t=\frac{1}{l} \tag{1}$$

B. Cryomicrotome Fluorescence Images

The scope of the research presented herein is focused on studying spatial variation of the total optical tissue attenuation coefficient across an entire organ.

The total optical tissue attenuation coefficient was measured from images produced by the cryomicrotome at the Dept. of Biomedical Engineering & Physics at the Academic Medical Center in Amsterdam, which provides micrometer-resolution images [3]. This is a novel application of the optical fluorescence images obtained with the cryomicrotome.

Given the unscattered collimated transmission T_c, which is the ratio of the intensity I of light exiting a slab of tissue of thickness t and the intensity I_0 of the light when it was first incident on the tissue slab, Beer's law can be used for calculating the total attenuation coefficient [5]:

$$T_c=\frac{I}{I_0}=e^{-\mu_t t}\Rightarrow\mu_t=-\frac{1}{t}\ln(T_c)=-\frac{1}{t}\ln\left(\frac{I}{I_0}\right) \tag{2}$$

The above scenario works only for a transmission geometry, wherein light enters and exits, without changing direction. However, the cryomicrotome setup is a reflection geometry, in which filtered excitation light is incident upon tissue and is reflected back as emission from the excited fluorophores embedded in the tissue [6], as shown in Fig. 1.

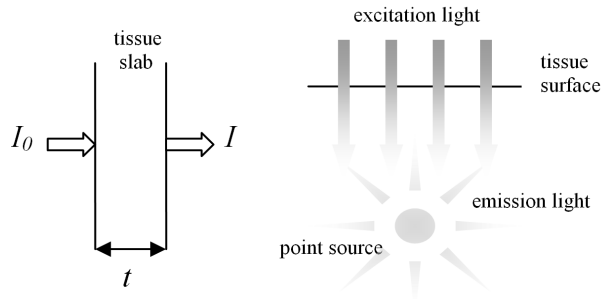

Fig. 1. Left figure: Transmission geometry showing a slab of tissue of thickness t on which light incident with intensity I_0 exits with reduced intensity I. Right figure: Reflection geometry of the cryomicrotome in which the excitation light is attenuated as it enters the tissue and the emission light reflected by the fluorescent point source is also attenuated.

To measure the total attenuation coefficient, the method of fitting a theoretical point spread function to the experimental images of fluorescent microspheres embedded in tissue is used. In this case, the theoretical point spread function is a model of the attenuation and distribution of light emitted by a point source in the turbid media of tissue.

This novel method for measurement of the total tissue attenuation coefficient is possible because the fluorescent microspheres of 15-micron diameter, when embedded in tissue via perfusion into the vasculature act as approximate point sources [6].

II. Method

At a radial distance r [μm], the intensity I of a point source with power I_0 radiating or emitting light isotropically is given by (see Rolf et al. 2008 for more detail [6]):

$$I(r) = I_0 \frac{e^{-\mu_t r}}{4\pi r^2} \tag{3}$$

The isotropic spread is modeled as a spherical intensity distribution of radius r. The light radiated isotropically by the point source is absorbed and scattered by the tissue, which is accounted for by the total attenuation coefficient μ_t in equation (3). Assuming homogeneous excitation, the attenuation of the excitation light, depending only on depth z, can be accounted for with an additional depth-dependent exponential factor in the tissue PSF model:

$$PSF_{tissue}(x,y,z) = I_0 \frac{e^{-\mu_t z} e^{-\mu_t r}}{4\pi r^2} \tag{4}$$

In the paper by Rolf et al. 2008 [6], it is assumed that the total tissue attenuation coefficient (which is the sum of the absorption and scattering coefficients) is identical for excitation and emission. However, according to measurements reported in Bishop et al. [2], the coefficients have differing values for excitation and emission, i.e. light attenuates differently when entering and exiting the tissue. The reason the attenuation coefficient differs from excitation to emission is because it is dependent on the wavelength of light, which is increased when it is emitted by the excited fluorochrome molecule, a phenomenon known as the Stokes shift. When a photon is absorbed by an atom, the latter enters an excited state with the gained energy. The atom relaxes to its ground state by emitting a photon at a lower frequency, i.e. longer wavelength. The Stokes shift indicates the energy dissipated by the atom [7]. Here, the PSF as presented by Rolf et al. 2008 [6] is adapted to incorporate the difference in optical tissue properties in regards to the attenuation of light. The improved theoretical PSF model now has two separate tissue attenuation coefficients, one for excitation (μ_{ex}) and the second for emission (μ_{em}):

$$PSF_t(x,y,z) = I_0 \frac{e^{-\mu_{ex} z} e^{-\mu_{em} r}}{4\pi r^2} \tag{5}$$

A. Fluorescence Microsphere Images

Images were obtained by preparing an excised porcine heart by perfusion with approximately 100,000 15-micron diameter FluoSpheres® carmine (excitation 582nm, emission 614nm) and red (excitation 570nm, emission 598nm) microspheres. Subsequently, the heart was immersed in a sodium solvent and thickening agent mixture, and frozen in the cryomicrotome. Excitation of both red and carmine microspheres was with 560±20 nm light. A digital camera captured an image of the longer-wavelength emission (635±30 nm) of both red and carmine microspheres coming from the cutting surface each time a slice of precise micrometer thickness was serially sectioned off from the frozen heart sample (see Fig. 2 for maximum intensity projection image). The image acquisition procedure is covered in more detail in [3, 6].

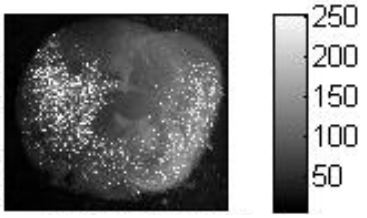

Fig. 2. Maximum intensity projection (MIP) of the 3D image stack (1351x1551x1464 voxel^3) of microspheres perfused in the porcine heart. MIP image dimensions of (1351x1551voxel^2), with voxel size of (50μm)^3.

B. Fitting the PSF to Microspheres

All the microsphere centerpoints in the porcine heart image data were detected by finding local maximum voxels. Dark current noise, hot voxels, and microsphere clusters, i.e. more than one microsphere embedded close together in the tissue, were precluded as follows: Only microspheres above a certain intensity threshold were extracted to avoid dark current. It was made sure that the microsphere's centerpoint was not a voxel with an average intensity above 100 across the entire depth to avoid hot voxels. Region growing out from the center voxel was performed to include only those neighbour voxels which had lesser intensity than the center voxel but higher intensity than the noise threshold, and it was made sure that the microsphere size was lesser than 14 voxels in all three dimensions to avoid microsphere clusters. Microspheres containing voxels with the saturated intensity of 255 in the 8-bit images were not included. This is because

the intensity information of saturated microsphere voxels is lost in the image acquisition. The 3D size of the analytical theoretical $PSF_t(x, y, z)$ model presented in equation (5) was set to match the size of the 3D extracted microsphere image. Unconstrained nonlinear optimization with the Nelder-Mead Simplex method [8] was used to obtain the optimal parameter values for the excitation and emission tissue attenuation coefficients for each microsphere by fitting the analytical theoretical $PSF_t(x, y, z)$ model (equation (5)) to each 3D extracted microsphere image. The cost function minimized was the mean square error between the theoretical $PSF_t(x, y, z)$ and the experimental $PSF_e(x, y, z)$:

$$\hat{o} = \arg\min_{o} \frac{1}{BWD} \sum_{x=1}^{B} \sum_{y=1}^{W} \sum_{z=1}^{D} [PSF_t(x,y,z) - PSF_e(x,y,z)]^2 \quad (6)$$

$$where \quad \hat{o} = \{\mu_{ex}, \mu_{em}\} \quad and \ PSF \ size \ [B,W,D]$$

III. Results

Over the entire 3D image stack of the porcine heart, the excitation and emission attenuation coefficients were calculated. Fig. 3 shows plots of the microspheres as points with the microsphere centerpoint intensity on the y-axis and the attenuation coefficient at that microsphere on the x-axis. Fig. 3 also shows the probability distributions of the coefficients. The scatter plots of Fig. 3 indicate the large range of variation in the tissue attenuation coefficients, which is consistently large for all bands of intensities of microspheres, i.e. the optical attenuation variation results are not influenced by microsphere intensity (see Table 1). Since carmine light is of longer wavelength than red light, it can penetrate deeper into tissue [9], i.e. intensity of carmine microspheres is brighter than red ones. In Fig. 3, the brighter microspheres were found to have smaller values of μ_{ex} and μ_{em}, so it is assumed that the first peak in both μ_{ex} and μ_{em} probability distributions correspond to carmine (brighter) and the second peaks to red.

Delaunay triangulation using the Quickhull algorithm [10] was employed for gridding of the tissue attenuation coefficient data for both excitation and emission. Tesselation-based linear interpolation was performed between the scattered data points by fitting a hypersurface of the form $s=f(x,y,z)$ to the data comprising of the spatial 3D locations (x, y, and z coordinates) of the microsphere centerpoints and the values of the tissue excitation and emission attenuation coefficients at those points. The result of the interpolation is shown in Fig. 4 as the map of spatial variation of μ_{ex} over the organ (microspheres are overlaid on the map as dots color-coded according to their μ_{ex} value).

A significant difference in the total optical tissue attenuation coefficient was observed between excitation and emission for both carmine (excitation – 13±4(1/mm) and emission – 9.4±3(1/mm)) and red (excitation – 29±5(1/mm) and emission – 25±5(1/mm)). A large range of values were observed for the tissue attenuation coefficient (24-34(1/mm) and 20-30(1/mm) for red excitation and emission, respectively; 9-17(1/mm) and 6.4-12.4(1/mm) for carmine excitation and emission, respectively), which intimates intramural variation of optical properties across the entire organ depending on light color.

Table 1. Variation in attenuation coefficient in porcine heart due to light wavelength, but it is not affected by the intensity of detected microspheres.

Color	Micro-sphere Intensity Band	Tissue Attenuation Coefficient (1/mm)			Light Wavelength (nm)		
		$\mu_{ex} \pm \sigma_{ex}$	$\mu_{em} \pm \sigma_{em}$	$\mu_{ex} - \mu_{em}$	λ_{ex}	λ_{em}	$\lambda_{em} - \lambda_{ex}$
Carmine	100-254	13±4	9.4±3	3.9	582	614	32
	100-140	14±4	10±3	4			
	140-180	13±4	9.6±4	3.4			
	180-220	13±3	8.8±3	4.2			
	220-254	13±3	9±3	4			
Red	100-254	29±5	25±5	4	570	598	28
	100-140	28±5	24±5	4			
	140-180	30±5	26±5	4			
	180-220	31±6	27±6	4			
	220-254	25±6	23±7	2			

IV. Conclusion

This proof-of-concept study indicates that intramural optical tissue attenuation properties may differ significantly throughout the tissue. A novel method of measuring the total optical tissue attenuation coefficient from fluorescence microsphere images was implemented for observing the pattern of spatial variation in optical tissue properties across a whole-organ. The fluorescent microspheres act as approximate point sources embedded in tissue that can be used as fiducial markers for attenuation coefficient measurements. Significant variation was demonstrated in optical tissue properties of a porcine heart that was filled with microspheres of two colors: carmine and red. A significant difference in the total optical tissue attenuation coefficient was observed between excitation and emission for both carmine and red. A large range of values were observed for the tissue attenuation coefficients. In addition, as shown in Fig. 4, there is a visible spatial pattern of intramural optical attenuation properties across the entire organ. This work will be extended in the future to study variation of the tissue attenuation coefficient in other organs such as lung and kidney, and other species like rat and human.

Although this proof-of-concept study indicates variation of optical tissue attenuation properties, further research is required before a global pattern of spatial variation of optical properties in intramural tissue can be verified. For instance, in the future the work will be improved by suppressing the spatial variation map in the heart cavity and other regions where there were no microspheres. In addition, the position of the microsphere with respect to the slicing affects the data points available for the PSF fitting. Thus, the microsphere position needs to be, in the future, incorporated in the PSF parameter optimization. For the PSF fitting, the minimum reached by the Nelder-Mead simplex optimization method is highly sensitive to the initial starting points (the user-defined initial values of the PSF parameters), and it may be resulting in a local minimum of the cost function (the mean square error between the theoretical PSF model and experimental microsphere image). Nonlinear bound-constrained (instead of an unconstrained method with initial starting points)

optimization will be tested in the future to reach the global minimum of the cost function and optimal values of the PSF parameters within a specified range, for quick convergence.

REFERENCES

[1] Shah, K., et al.: Molecular Optical Imaging: Applications Leading to the Development of Present Day Therapeutics. NeuroRX 2(2), 215--225 (2005)

[2] Bishop, M., et al. The Role of Photon Scattering in Optical Signal Distortion during Arrhythmia and Defibrillation. Biophys. J. 93(10), 3714--3726 (2007)

[3] Spaan, J., et al.: Visualisation of Intramural Coronary Vasculature by an Imaging Cryomicrotome Suggests Compartmentalisation of Myocardial Perfusion Areas. Med. Biol. Eng. Comp. 43, 431--435 (2005)

[4] Wilson, B. C., et al.: Optical Reflectance and Transmittance of Tissues: Principles and Applications. IEEE J. Quant. Elect. 26(12), 2186--2199 (1990)

[5] Cheong, W. F., et al.: A Review of the Optical Properties of Biological Tissues. IEEE J. Quant. Elect. 26(12), 2166--2185 (1990)

[6] Rolf, M.P., et al.: Diameter Measurement from Images of Fluorescent Cylinders Embedded in Tissue. Med. Biol. Eng. Comput. 46, 589--596 (2008)

[7] Guilbault,G. Practical Fluorescence, 2nd ed. CRC (1990)

[8] Lagarias, J., et al.: Convergence Properties of the Nelder-Mead Simplex Method in Low Dimensions. SIAM J. of Opt. 9(1), 112--147 (1998)

[9] DaCosta, R. S., et al.: Optical Techniques. Ch. 44 of Colonoscopy, ed. J. D. Waye, et al., Wiley-Blackwell, page 511 (2003)

[10] Barber, C., et al.: The Quickhull Algorithm for Convex Hulls. ACM Trans. Math. Soft. 22(4), 469--483 (1996)

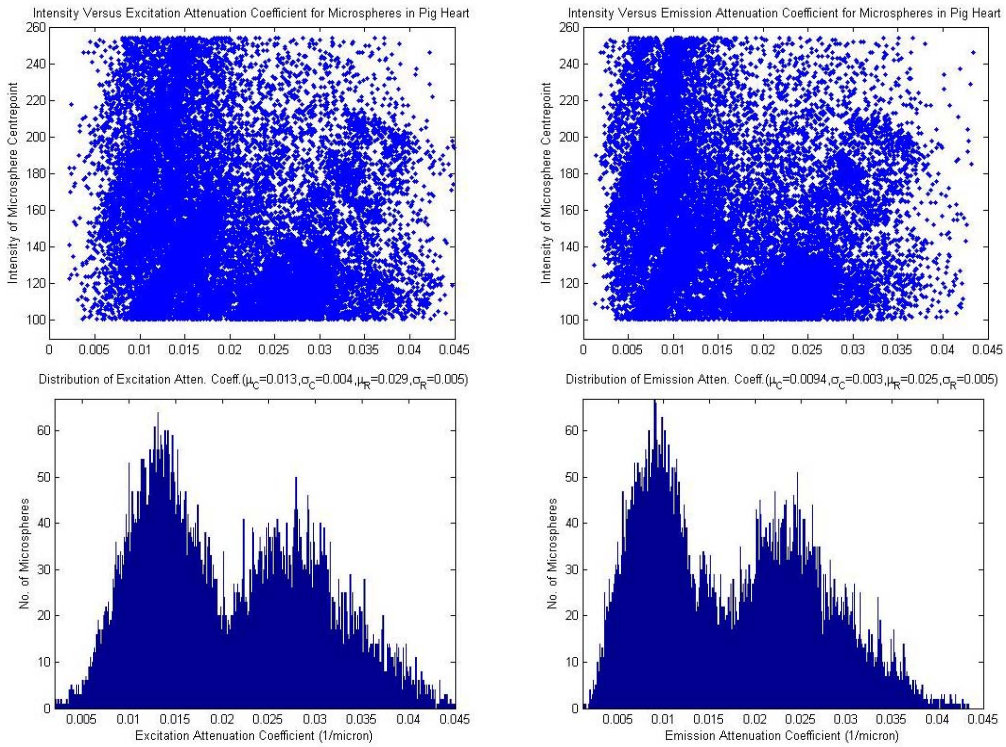

Fig. 3. Microspheres depicted as points in the microsphere-centrepoint-intensity versus tissue attenuation coefficient plot (upper). Probability distributions (lower) of the excitation (left) and emission (right) attenuation coefficients, with units of [1/μm]. Above scatter plots indicate the large range of variation of tissue attenuation properties across entire porcine heart (tissue attenuation variation is independent of microsphere intensity).

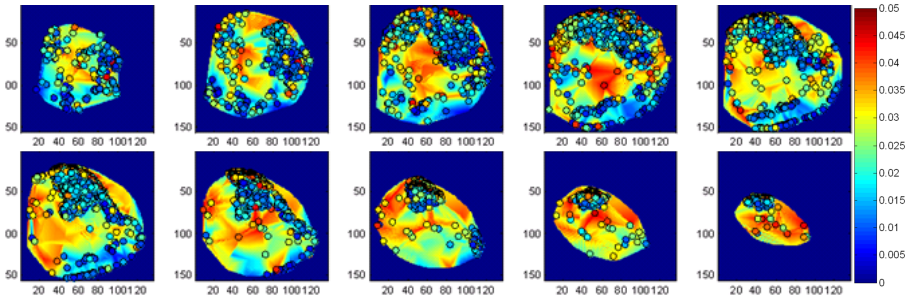

Fig. 4. Short-axis views across entire heart showing the spatial variation in μ_{ex}. Colorbar represents the range (1/μm). Each slice is 7.5 mm deeper in the long axis from base to apex (from upper left to bottom right). Image dimensions: 7x8 cm^2. Microspheres (colored, based on μ_{ex}) are superimposed.